International Journal of Applied Glass Science

RESEARCH ARTICLE OPEN ACCESS

Modeling of Physical–Chemical and Thermomechanical Properties of Glasses From Recycled Waste

Roberto Ercoli[1] | Paola Stabile[1] | Gabriele Giuliani[1] | Michael R. Carroll[1] | Gianluca Bianchini[2] | Eleonora Paris[1]

[1]School of Science and Technology, Geology Division, University of Camerino, Camerino, Italy | [2]Department of Physics and Earth Sciences, University of Ferrara, Ferrara, Italy

Correspondence: Paola Stabile (paola.stabile@unicam.it) | Gabriele Giuliani (giuliani.gabriele91@gmail.com)

Received: 9 December 2025 | **Revised:** 10 February 2026 | **Accepted:** 26 February 2026

Keywords: construction and demolition waste (CDW) | glasses | thermomechanical performance | vitrification

ABSTRACT

This research focuses on understanding the high-temperature phase evolution occurring during the vitrification of heterogeneous construction and demolition wastes (CDWs). The aim of this project is to transform this widely distributed and mostly unused waste stream into a homogeneous, engineered, glass-based material with predictable properties, valuable for the glass industry. Starting with vitrification experiments, CDW samples (< 63 μm) were heated to target temperatures (*T*) of 1100°C, 1200°C and 1300°C and held isothermally for either 2 or 8 h. The experimental products were chemically characterized by electron microprobe (EMP) analysis, and the results show that the SiO_2- and Al_2O_3-rich samples (RAS and PRO) achieved a high degree of vitrification at ~1300°C, forming a homogeneous glassy matrix. Conversely, the high CaO content in the TAL sample hindered complete vitrification by promoting the stability of calcium-rich crystalline phases (e.g. larnite) up to temperatures as high as 1600°C, as shown by x-ray diffraction patterns on the treated samples. Building on these findings, the GlassNet model was employed to design a blend of PRO sample with the addition of fly ash (FA.REI) and glass waste (VF3) to improve thermomechanical performance. The model predicted an optimized mixture (Exp.a), fully composed of waste materials, for acoustic and thermal insulation applications, thus demonstrating waste recycling potential for producing new high-performance materials with practical applications.

1 | Introduction

Construction and demolition waste (CDW), originating from buildings restauration, reconstruction, or demolition, represents one of the largest waste streams globally. In the European Union, CDW accounts for more than 30% of all generated waste, posing significant environmental and management challenges [1]. In response to this issue, European directives, in line with the principles of the circular economy, are pushing for a drastic reduction in landfilling in favor of recycling and, ideally, "upcycling," that is, converting waste into new products of higher value. However, conventional recycling of CDW is often hindered by its inherent chemical and mineralogical heterogeneity [2–7]. This variability stems from the diverse range of building materials used, different construction ages, and varying demolition practices. Such heterogeneity complicates separation processes and limits the use of recycled fractions in high-performance applications, often confining them to low-value uses such as backfilling and road base fills [8–10].

In this context, vitrification emerges as a promising valorization technology, as an opportunity to produce high-value glass products while recycling unused waste. This thermal process involves melting the waste at high temperatures (typically > 1100°C) [6, 7, 11, 12] and then quenching the molten mass to obtain a predominantly amorphous, glass-rich product. The advantages of vitrification are manifold: it allows for the treatment of a heterogeneous waste stream, transforming it into a

homogeneous, inert, and long-term stable product. The resulting vitrified material can find application as a secondary raw material for producing tiles, glass ceramics, high-quality aggregates, glass fibers, or insulation materials, but also for applications in the confinement of hazardous/radioactive elements [13, 14].

The success of the vitrification process and the properties of the final product are strictly dependent on three key factors: (i) the chemical composition of the starting material, (ii) the treatment temperature, and (iii) the isothermal dwell. In particular, the balance between abundances of network formers (e.g., SiO_2, Al_2O_3) and fluxing/network-modifying oxides (e.g., CaO, Na_2O, K_2O) controls the melting temperature, melt viscosity, working range, and crystallization kinetics during cooling [11, 15, 16]. For example, elevated CaO contents can lower the melting point but can also stabilize refractory Ca-rich crystalline phases, potentially hindering the formation of a fully homogeneous glassy product [13, 17].

The primary objective of this work is to establish a methodological framework for a possible upcycling process of highly heterogeneous CDW. The investigation has been carried out by vitrification experiments aimed at the production of glass and glass-ceramic materials, obtained via mixing CDW with other waste materials streams. Starting with a mineralogical–chemical characterization of the wastes, a combination of high-temperature experiments has been merged with predictive modeling (GlassNet) to rationally design optimal mixes necessary to produce glass and glass-ceramic materials with desirable composition and performance. An experimental composition (Exp.a) is presented as a proof-of-concept case study, demonstrating how the proposed methodology can be applied to design a fully waste-derived glass with targeted thermomechanical properties.

For this purpose, here, we systematically explore how CDW compositional variations may influence their vitrification behavior at various temperatures (1100°C–1600°C) and dwell times (2 and 8 h). In addition, this work adopts a composition-informed approach that moves beyond simple characterization. Leveraging knowledge of a given CDW's composition and physical properties, we use predictive modeling tools (e.g., GlassNet) [18] to rationally design new blends, even from heterogeneous waste streams. Specifically, we formulate mixtures of CDW with coal fly ash (FA.REI) and a glass-cutting by-product (VF3) to maintain a fixed melting temperature while enhancing thermomechanical performance. This composition–process–property framework aims to enable reproducible upcycling of mixed CDW into higher-value glass and glass-ceramic products.

2 | Methods

2.1 | Starting Materials

Three distinct types of CDW were used in this study, designated as RAS, PRO, and TAL, collected from different disposal sites of the rubble related to the 2016 earthquakes in Central Italy. Chemical and mineralogical data for the samples used in this study are reported in Table 1. A detailed characterization of a wide range of CDW samples from the earthquake area is reported in [19], highlighting the chemical/mineralogical variability among the samples analyzed, with a view toward possible recycling. To ensure a homogeneous starting material for the vitrification experiments, a representative quantity of the size fraction smaller than 8 mm of each CDW sample was sieved to obtain a fine powder with a particle size of less than 63 μm. This grain size was selected for different reasons: (i) the finest CDW fractions currently have no recycling routes and are typically landfilled; (ii) when collected on site, this fine fraction requires no additional grinding, possibly allowing a cost reduction at the industrial scale.

TABLE 1 | Chemical compositions (wt.%) of starting waste samples determined by EMPA and phase abundances (wt.%) in CDW by XRPD ([20, 21] described in the text, Section 2.3.2).

	RAS	PRO	TAL	FA.REI25	VF3
SiO_2	34.00	35.71	15.89	57.71	64.01
Al_2O_3	8.23	7.37	3.41	21.24	2.83
Fe_2O_3	3.38	2.85	1.44	7.96	2.72
MnO	0.08	0.08	0.06	0.08	0.08
MgO	1.75	1.99	1.28	2.65	3.85
CaO	28.98	25.23	39.31	5.16	15.26
Na_2O	0.70	1.15	0.29	0.93	10.12
K_2O	1.57	1.29	0.58	2.44	0.65
TiO_2	0.40	0.40	0.18	1.16	0.43
P_2O_5	0.14	0.16	0.10	0.67	0.05
LOI	20.90	22.83	32.02	—	—
Total	100.10	99.06	94.56	100.00	100.00
Amorphous	45.0	48.3	18.5	n.d.	n.d.
Calcite	37.5	36.8	66.1	n.d.	n.d.
Quartz	12.5	13.6	9.0	n.d.	n.d.
Gypsum	4.3	0.0	6.5	n.d.	n.d.
Albite	0.0	0.4	0.0	n.d.	n.d.
Illite	0.7	0.0	0.0	n.d.	n.d.
Zeolite	0.0	0.9	0.0	n.d.	n.d.

Abbreviation: n.d. = not determined.

In the second part of the study, focused on computational modeling, two additional industrial by-products were taken into consideration: a fly ash (FA.REI) and a glass cutting waste (VF3) (Table 1). The glass cutting waste VF3 has been collected from Fabriano (AN; Italy) while the coal fly ash (FA.REI) is from ENEL's Torrevaldaliga Nord's coal-fired power plant (Civitavecchia, RM; Italy). These waste materials were selected to be blended with PRO sample to design new products with tailored properties characterized by good thermal and acoustic insulation capabilities (discussed below).

2.2 | Synthesis of Glasses and High-Temperature Experiments

The thermal treatments were performed in a laboratory high-temperature furnace (Nabertherm LHT02/17) under ambient air

fugacity. For each run, the CDW powders were placed in a Fe-saturated Pt crucible (used for previous exploratory experiments with the same materials under similar conditions) and heated to the target temperatures of 1100°C, 1200°C and 1300°C over the course of 3 h. The sample was then kept at the final temperature for two different dwell times of 2 and 8 h and then quenched with a rate > 500°C min^{-1}. An additional experiment was performed on the TAL sample at 1600°C to investigate its behavior at higher temperatures.

2.2.1 | Computational Modeling and Optimization

To design a novel blend with targeted properties, a computational approach was adopted using GlassNet [18], a machine learning model for predicting glass properties from its composition. GlassNet is used within the compositional domain spanned by its training database (SciGlass), which comprises more than 218 000 glass compositions across the main oxide glass species (e.g., silicate, borosilicate, aluminosilicate, and related industrial glasses). The simulation aimed to identify the optimal component proportions that preserve the melting temperature (T_m) and thus the energy demand, as well as the associated environmental impact of the melting stage, while enhancing thermomechanical performance.

These improved properties are particularly advantageous in high-performance glass, where resistance to mechanical stress and thermal cycling enhances longevity. A new composition was designed by blending CDW.PRO_63 with fly ash (FA.REI) and glass waste (VF3).

For the sake of simplicity, if $w = [w1, w2, w3]$ is the vector of weight fractions for CDW.PRO_63, FA.REI, and VF3 respectively, and P is the property matrix of the raw components, the property vector of the mixture, Pmix, is calculated by Equation (1):

$$P\text{mix} = w \cdot P \tag{1}$$

A multi-objective function, $F(w)$, was formulated to be minimized. The function was designed to simultaneously minimize thermal conductivity (TC^{mix}) while maximizing Young's modulus (E^{mix}), shear modulus (G^{mix}), and thermal shock resistance (TSR^{mix}), as shown in Equation (2):

$$\min_w F\ (w) = \min_w \left(TC^{mix} - TSR^{mix} - E^{mix} - G^{mix}\right) \tag{2}$$

This optimization was performed subject to a series of constraints. Two equality constraints were imposed: (i) the sum of the weight fractions must equal one, as in Equation (3):

$$\sum_{i=1}^{3} w_i = 1 \tag{3}$$

and (ii) the melting temperature of the mixture (T_m^{mix}) must be equal to that of the parent CDW.PRO (T_m^{target}) as shown in Equation (4):

$$T_m^{mix} = \sum_{i=1}^{3} w_i\, P_{i,\,T_m} = T_m^{target} \tag{4}$$

Furthermore, a set of inequality constraints was established to ensure physically meaningful proportions and to maintain a hierarchical composition where the CDW content is the highest and the glass waste content is the lowest: $w1 \geq w2 \geq w3 \geq 0$. This constrained optimization problem was solved using the "scipy.optimize.minimize" function from the SciPy library in Python [18], which iteratively finds the weight vector w that satisfies all constraints while minimizing the objective function.

2.3 | Samples Characterization

2.3.1 | Microchemical Analysis

The chemical composition of the thermally treated samples was investigated in detail using a JEOL JXA-8200 Electron Microprobe, operating at an accelerating voltage of 15 kV and a beam current of 5 nA. The samples were coated with graphite as a conductive material. The standard materials used for quantitative WDS analyses consisted of a range of silicate and oxide minerals of composition similar to the studied compositions, such as omphacite, grossularite, fayalite, rhodonite, K-feldspar, olivine, and fluorapatite. Back-scattered electron (BSE) images of the samples were also collected during microprobe analyses and examples are reported in Section 3.

2.3.2 | X-Ray Diffraction

The mineralogical composition of the treated samples of CDW (PRO, RAS, and TAL) was determined using a Philips PW1060/81 powder diffractometer (Cu Kα radiation, λ = 1.5418 Å, 40 kV, 25 mA). Analyses were run over a 2θ range of 5°–70°, with a step size of 0.02° and a dwell time of 1 s per step. Mineral phases were identified by using the Match! Software [20] and RRUFF Reference database [21]. To quantify both the crystalline phases and the amorphous content, Rietveld refinement on the diffraction patterns using a profile matching phase was performed. For quantification, a mixture of 0.5 g of the sample and 0.05 g of corundum (Al_2O_3), used as an internal standard, was analyzed. Uncertainties on the semi-quantitative x-ray diffraction (XRD) data are ca. ± 2 wt.%.

2.3.3 | Leaching Tests

To evaluate the potential metal release and the overall environmental compatibility of the materials, leaching tests were performed following the UNI EN 12457-2:2004 protocol [22]. Powdered samples were mixed with deionized water at a liquid-to-solid ratio (L/S) of 10:1 and agitated for 24 h. After equilibration, the suspensions were centrifuged using a NEYA 8 centrifuge (4000 rpm, 10 min) and subsequently filtered through 0.45 µm cellulose acetate syringe filters. The resulting leachates were then analyzed for trace elements by ICP-MS (iCAP, TQ, Thermo Fisher Scientific).

3 | Results and Discussion

3.1 | Chemical and Mineralogical Characterization of Starting Materials

The chemical compositions of the three starting CDW samples are reported in Table 1 [19]. The RAS and PRO samples exhibit

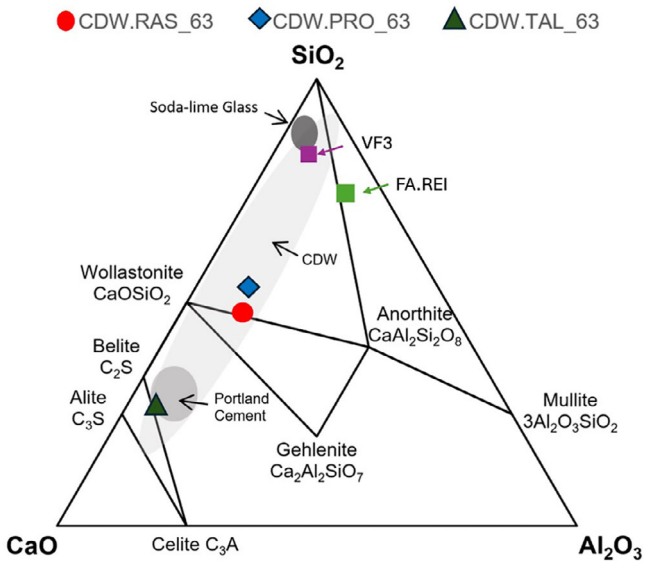

FIGURE 1 | Composition of the three samples (CDW.RAS_63, CDW.PRO_63, and CDW.TAL_63) plotted on the CaO-Al_2O_3-SiO_2 ternary diagram, showing their position relative to the stability fields of major silicate and aluminosilicate phases. CDW from the literature is also shown as light gray area ([25] and references therein), along with Portland cement in medium gray [23] and soda lime glasses in dark gray areas [26].

similar compositions, characterized by high concentrations of SiO_2 at ~34 and ~36 wt.%, respectively, and Al_2O_3 at ~8 and ~7 wt.%. In sharp contrast, the TAL sample was chosen as it is significantly depleted in these glass-forming oxides, with only ~16 wt.% SiO_2 and ~3 wt.% Al_2O_3, but is enriched in calcium oxide (CaO), reaching ~39 wt.%, compared to ~29 wt.% in RAS and ~25 wt.% in PRO. These compositional differences are presented in the CaO–Al_2O_3–SiO_2 ternary diagram (Figure 1). In the ternary plot, TAL falls deep within the high-CaO corner of the diagram, in proximity to the stability fields of alite (C_3S) and belite (C_2S), phases characteristic of Portland cement clinker, which are known for their high melting points [23, 24]. Conversely, PRO and RAS fall in an area less rich in CaO. This compositional distinction is directly related to the different source of the CDW, influenced by provenance from areas with different building stones (limestones, travertine, sandstones, decorative stones), ceramic materials (tiles, rooftiles, bricks, sanitaryware), concrete, and plasters. The relative quantities of these different components control bulk composition and therefore the different responses to the thermal treatments [3, 6].

3.2 | Phase Evolution and Vitrification Behavior

The response of the CDW samples to the thermal treatments is directly correlated with their initial chemical composition. Major oxide compositions of the vitrification CDW products are reported in Table 2. For the silica- and alumina-rich samples, increasing the temperature and dwell time promotes progressive melting and vitrification.

At 1100°C, the samples showed macroscopically only initial signs of sintering. At 1200°C, significant sintering and partial melting were observed, with the particles beginning to weld together. Finally, at 1300°C, both at 2 and 8 h, RAS and PRO (Figure 2a,b, respectively) transformed into a dark, apparently homogeneous, glassy materials, suggesting significant vitrification. In contrast, the high-calcium TAL composition (Figure 2c) demonstrated significant resistance to vitrification. Despite heat treatment at 1300°C for 8 h, the material retained a powdery, sintered morphology and showed no macroscopically visible glass formation.

The more efficient vitrification of RAS and PRO compared to TAL is related to their favorable bulk composition, rich in glass-forming oxides (SiO_2 and Al_2O_3), which readily form a stable amorphous network upon melting and rapid quenching. In addition, quantitative XRPD analysis (Table 1) on the starting CDW samples corroborates these observations, reflecting higher starting amorphous contents in RAS and PRO in comparison with TAL sample (45 and 48 vs. 18 wt.%, respectively). BSE images of all the experimental samples (Figure 3) show the morphological evolution of the CDW samples as a function of increasing temperature and dwell time. Both PRO and RAS exhibit comparable behavior: i.e. they show amorphous component at longest dwell times and higher temperature, consistent with their similar compositions. In contrast, the TAL sample, reflecting its different chemical and mineralogical composition (Table 1), shows solid-state recrystallization with no evidence of vitrification, even at 1300°C (Figure 3m–r). To further investigate possible vitrification of the TAL sample, an additional experiment at 1600°C was performed, but the resulting sample is still crystalline, containing < 60%–70% glass based on optical examination. The observed behavior of the TAL sample might be useful in the future if we consider more refractory-oriented applications.

At 1100°C (Figure 3a,b), the materials in PRO retain a granular and highly porous microstructure for both dwell times. They appear as aggregates of distinct particles with minimal interaction or welding between them. This indicates that at this temperature, only initial solid-state sintering has occurred, without the formation of a significant melt phase. A significant transformation is observed at 1200°C (Figure 3c). Here, the formation of a substantial liquid (glassy) phase is evident (darker gray material in Figure 3c). This is characterized by two key features: the pores lose their angular shape and become rounded and more isolated, and a new cohesive matrix begins to form, engulfing the residual crystalline grains (visible as brighter phases). The samples treated for 8 h (Figure 3d) show a more advanced state of densification and homogenization compared to their 2-h counterparts. Finally, at 1300°C (Figure 3e,f), the vitrification process is effectively complete for both CDW types. The microstructure is now dominated by a homogeneous and continuous glassy matrix, which appears largely featureless in the SEM images. The porosity has been drastically reduced to a few small, isolated, spherical voids at lower duration, and the original crystalline particles have been almost entirely dissolved into the melt. An analogue situation can be observed for RAS experimental samples in which the microstructure turns more homogeneous and glassier with increasing melting temperature and duration. Overall, the samples are more porous and microcrystalline at the lower temperature of 1100°C and 1200°C (Figure 3g–i). Looking at the TAL sample, temperature and experimental time do not affect the vitrification process since the materials show a clear presence

TABLE 2 | Glass chemical composition of the experimental products, obtained by electron microprobe analyses. 1-sigma standard deviations (stdev) are also reported below each phase when 5–10 measurements have been carried.

Sample	Phase	SiO_2	Al_2O_3	Na_2O	SrO	MnO	K_2O	MgO	SO_3	FeO	CaO	P_2O_5	TiO_2	BaO	Cr_2O_3	Total
PRO-1100-2	Glass	61.71	17.42	5.67	0.05	0.04	8.06	0.48	0.03	1.23	4.98	0.04	0.18	0.09	0.01	100.00
	stdev	5.52	0.47	0.82	0.07	0.04	2.09	0.4	0.04	1.36	4.43	0.05	0.25	0.04	0.01	
PRO-1100-8	Glass	72.69	3.97	4.70	0.05	0.20	6.18	2.07	0.01	3.66	6.19	0.03	0.16	0.06	0.01	100.00
	stdev	3.78	1.07	0.46	0.09	0.06	0.25	0.61	0.01	1.46	0.70	0.04	0.11	0.04	0.03	
PRO-1200-2	Glass	71.61	3.76	2.65	0.02	0.10	7.56	2.10	0.06	2.09	9.72	0.07	0.22	0.02	0.02	100.00
	stdev	4.35	2.69	0.19	0.03	0.05	0.95	0.33	0.05	0.51	1.03	0.03	0.13	0.03	0.02	
PRO-1200-8	Glass	61.52	8.01	3.03	0.07	0.13	8.32	3.65	0.13	3.25	11.26	0.15	0.38	0.09	0.02	100.00
	stdev	2.44	1.89	0.14	0.08	0.03	0.37	0.68	0.14	0.43	0.44	0.04	0.13	0.06	0.03	
PRO-1300-2	Glass	45.75	9.75	1.58	0.03	0.09	1.85	2.62	0.03	3.64	33.67	0.43	0.52	0.01	0.03	100.00
	stdev	0.14	0.09	0.05	0.04	0.03	0.04	0.07	0.02	0.13	0.22	0.05	0.03	0.01	0.03	
PRO-1300-8	Glass	46.44	9.30	1.56	0.05	0.11	1.68	2.57	0.00	3.27	34.08	0.41	0.49	0.02	0.03	100.00
	stdev	0.10	0.13	0.07	0.07	0.02	0.03	0.08	0.00	0.08	0.16	0.03	0.04	0.03	0.03	
RAS-1100-2	Glass	74.43	5.48	0.88	0.00	0.05	9.91	0.77	0.03	2.02	5.26	0.07	0.94	0.11	0.04	100.00
	stdev	4.24	4.59	0.11	0.00	0.01	0.58	0.51	0.04	0.81	2.80	0.03	0.78	0.02	0.05	
RAS-1100-8	Glass	74.79	1.77	2.01	0.02	0.13	9.00	0.73	0.09	1.31	9.60	0.09	0.14	0.30	0.02	100.00
	Stdev	3.29	0.54	0.14	0.04	0.04	2.04	0.23	0.05	0.34	1.33	0.06	0.04	0.18	0.02	
RAS-1200-2	Glass	73.07	2.31	1.94	0.01	0.10	9.02	1.12	0.04	1.47	10.62	0.08	0.15	0.07	0.00	100.00
	Stdev	2.20	0.58	0.13	0.03	0.04	1.53	0.23	0.03	0.17	0.42	0.04	0.06	0.09	0.01	
RAS-1200-8	Glass	73.75	1.42	2.03	0.02	0.11	8.67	1.08	0.05	1.40	11.19	0.07	0.14	0.06	0.01	100.00
	Stdev	2.72	0.39	0.15	0.03	0.04	1.57	0.24	0.04	0.30	0.51	0.02	0.05	0.05	0.01	
RAS-1300-2	Glass	42.20	9.53	0.93	0.06	0.10	1.84	2.33	0.04	3.81	38.17	0.40	0.52	0.02	0.03	100.00
	stdev	0.28	0.15	0.05	0.07	0.05	0.02	0.05	0.04	0.07	0.14	0.04	0.05	0.03	0.03	
RAS-1300-8	Glass	42.18	9.53	0.91	0.04	0.10	1.75	2.32	0.02	3.79	38.42	0.38	0.51	0.02	0.02	100.00
	stdev	0.12	0.15	0.03	0.06	0.04	0.03	0.07	0.02	0.04	0.11	0.03	0.04	0.02	0.03	

Note: All analyses normalized to 100% totals to facilitate comparison. Original analysis totals were between 97.5 and 100.1 wt.%.

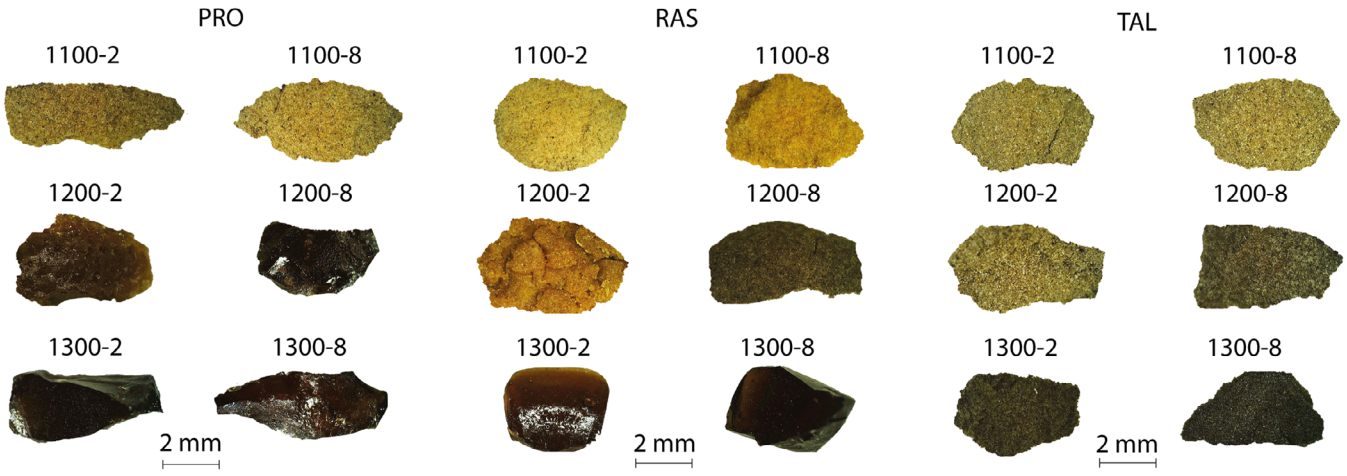

FIGURE 2 | Macroscopic appearance of the RAS, PRO, and TAL samples after thermal treatment at 1100°C, 1200°C, and 1300°C for 2 and 8 h, showing the progression from sintered powder to a vitrified product.

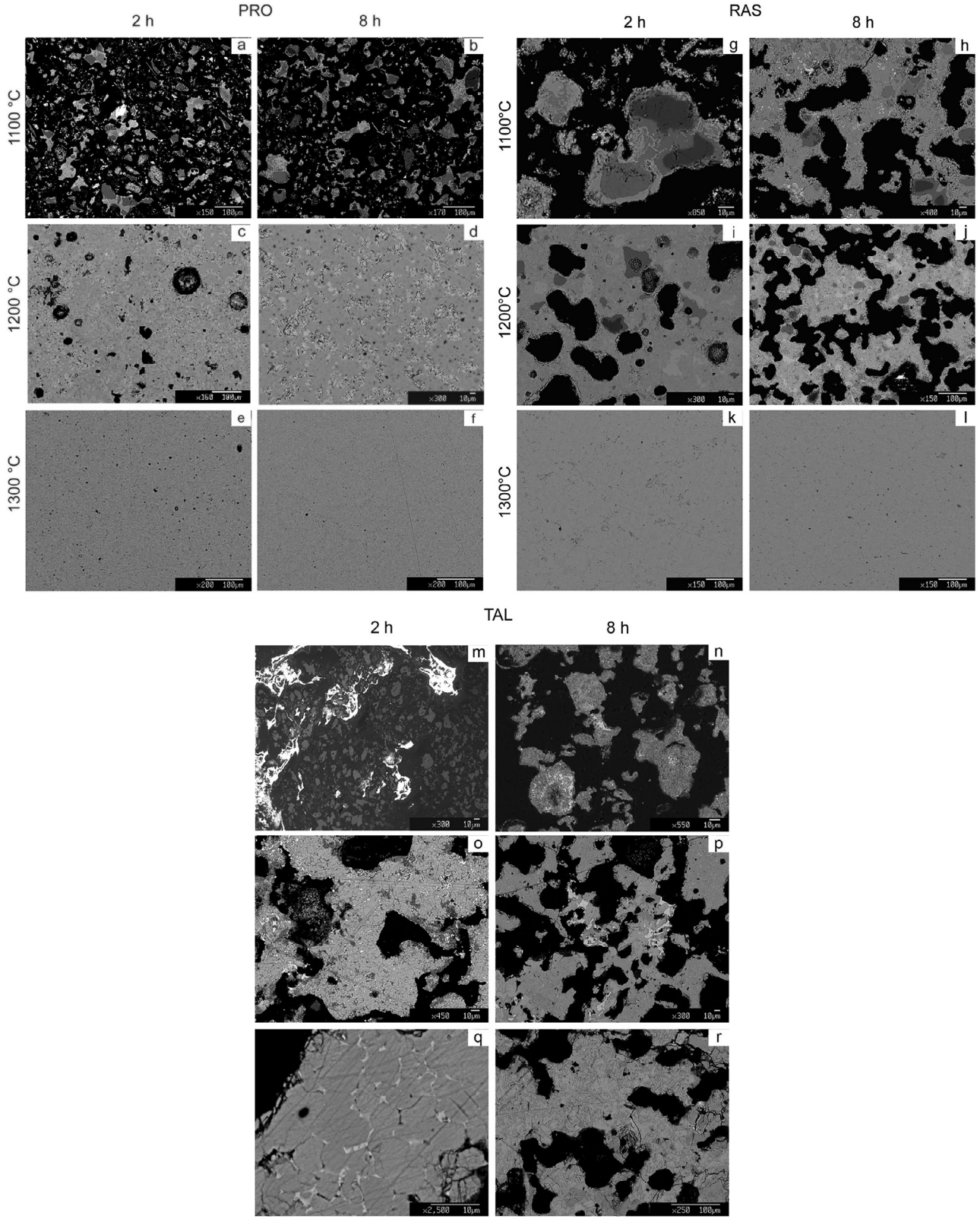

FIGURE 3 | Back-scattered electron (BSE) images of the experimentally produced samples (a–f) PRO, (g–l) RAS, and (m–r) TAL, as function of temperature (1100°C, 1200°C, and 1300°C) and dwell time (2 and 8 h). Differences in scale in some images were necessitated by differences in the sample material available.

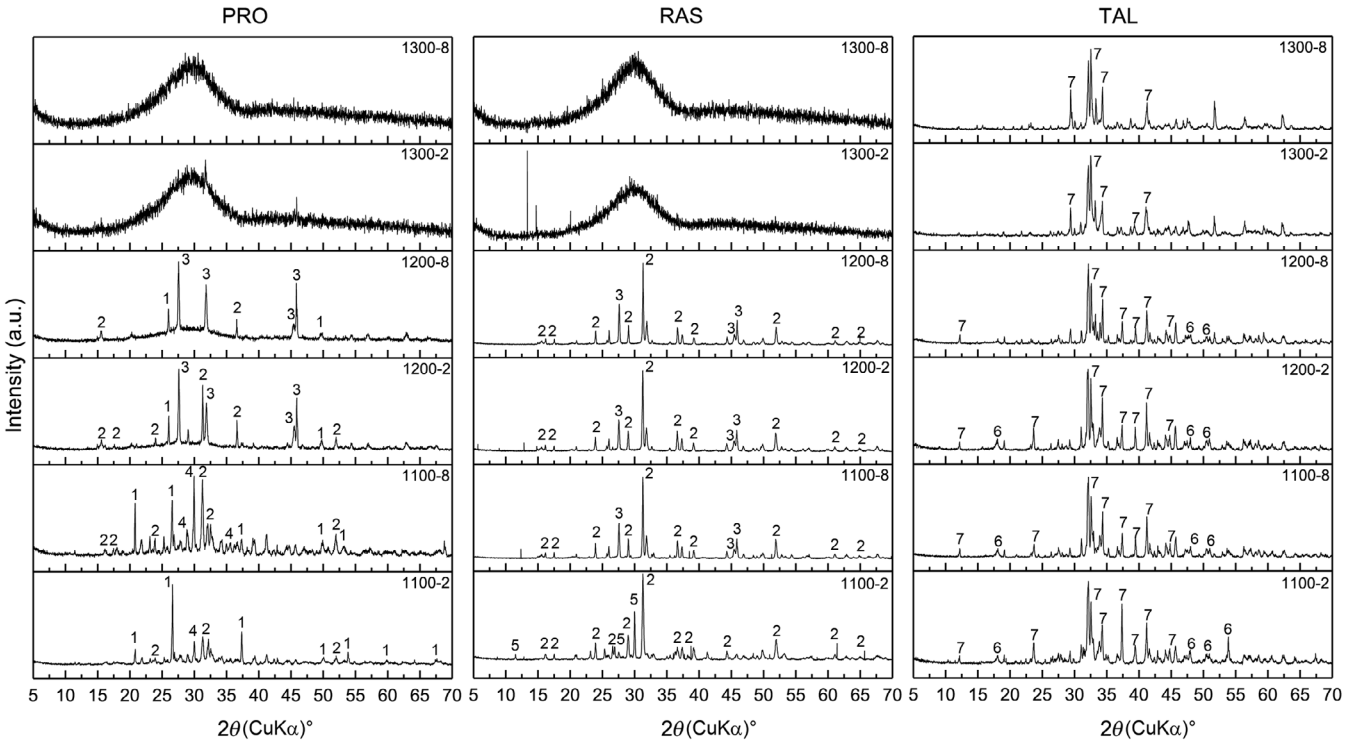

FIGURE 4 | XRPD patterns of the experimental products. Numbers indicate the following phases: 1 = quartz, 2 = melilite, 3 = pseudowollastonite, 4 = clinopyroxene, 5 = wollastonite, 6 = portlandite, and 7 = larnite. Numbers in the upper right corner of each panel show T (°C) and dwell time (h).

of crystalline component even at the longest duration and the highest melting temperature of 1300°C (Figure 3q,r), although a formation of liquid (glass) phase becomes more evident in the sample at 1300°C from 2 h (Figure 3q) where the interstitial glass is evident from the BSE image in the areas occurring between the crystalline domains. Despite such evidence, electron microprobe analysis (EMPA) could not be performed on these areas to determine the glass chemical composition of the sample owing to the presence of contaminating Ca-rich crystalline phases; chemical information are, therefore, not reported along with the other RAS and PRO products in Table 2.

Concerning the influence of experimental dwell times (2 or 8 h), the analytical data reveal that its effect is generally secondary to that of temperature. At the highest temperature of 1300°C for the well-vitrifying RAS and PRO samples, extending the treatment from 2 to 8 h has a negligible impact on the final products that turn completely glassy regardless of the experimental melting duration. This indicates that the vitrification kinetics are rapid once a sufficiently high temperature is reached; thus, they are more affected by temperature and composition than by time. However, time plays an important role on chemical homogeneity of glasses and longer experimental durations, as well as higher temperatures, produce more chemically homogeneous glass in the samples analyzed (see standard deviations [SD] on glass analyses in Table 2).

The temperature influence on the presence of glass and crystalline phases of the three samples is also evident in Figure 4, where the XRPD patterns of all the treated samples are shown.

At the lower temperatures (1100°C and 1200°C), the main crystalline phases present in PRO samples are quartz (SiO_2), melilite mainly as the Ca- and Al- rich member gehlenite ($Ca_2Al(AlSiO_7)$), pseudowollastonite ($CaSiO_3$) or beta-wollastonite, which is the high-temperature ambient-pressure polymorph of wollastonite, stable above ca. 1125°C [27] and clinopyroxene, mainly diopside ($CaMgSi_2O_6$). Gehlenite is a high-temperature phase forming in ceramics and it is common in heterogeneous waste materials at high temperature, like municipal solid waste bottom ash [12, 28]. The structure of gehlenite can incorporate the Al_2O_3 present in CDW and can also include transition elements, suggesting it might serve as a possible confinement phase for other metals [3]. At the higher temperature of 1300°C, already at 2 h, the PRO sample clearly shows only the presence of glass, corroborating the observations from BSE images. RAS samples show some similar mineralogical features marked by the presence of gehlenite, wollastonite at lower temperature, and pseudowollastonite from 1100°C and 8 h as experimental conditions, and evidence of completely amorphous samples at 1300°C. In contrast to the PRO products, RAS do not present any quartz crystals or clinopyroxene at lower temperatures. The mineralogical features are completely different in TAL samples, which show only calcium-rich phases typically found as cement components, that is, portlandite, which is calcium hydroxide ($Ca(OH)_2$) formed as a secondary phase after CaO because hydration and carbohydration processes are expected to occur after thermal treatment, and larnite, a Ca-bearing silicate specie (Ca_2SiO_4). Larnite is the natural mineral species whose structure corresponds to the synthetic β-Ca_2SiO_4, forming as belite in Portland cement. The name larnite is connected to a series of Ca_2SiO_4 polymorphs (γ, β, α in order of increasing temperature

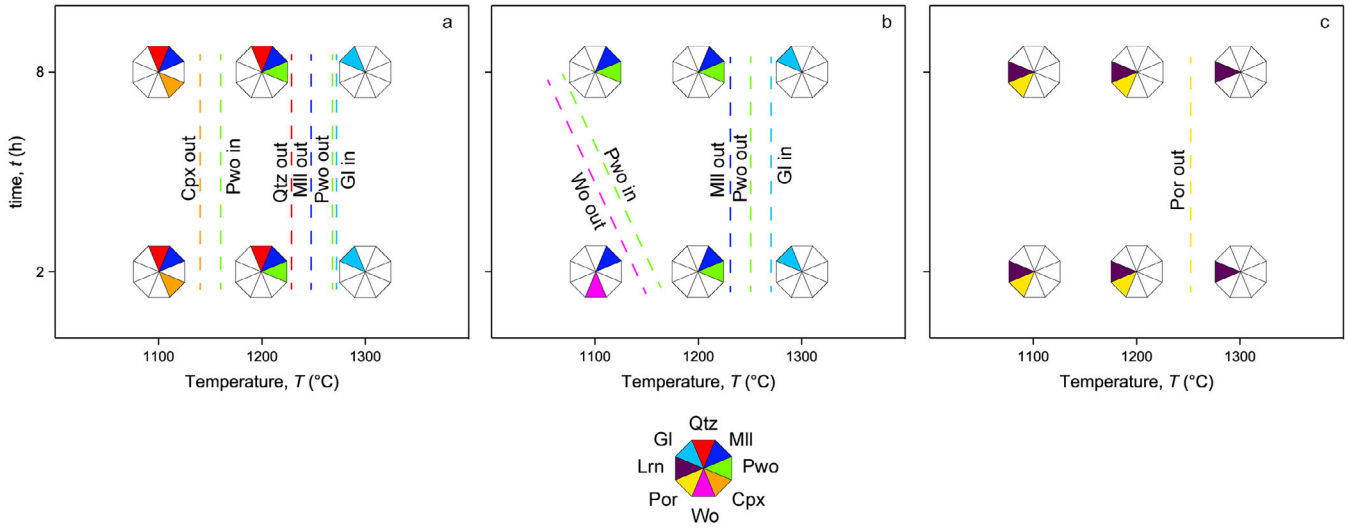

FIGURE 5 | Phase relations as a function of temperature and dwell time in PRO (a), RAS (b), and TAL (c) experimental samples. Cpx = clinopyroxene, Gl = glass, Lrn = larnite, Mll = melilite, Por = portlandite, Pwo = pseudowollastonite, Qtz = quartz, Wo = wollastonite.

of stability) where β and α phases are characterized by reversible polymorphic transitions and α presents also a higher and a lower temperature phase [29], difficult to detect because of peak overlapping in the XRPD patterns of quenched samples. The persistent presence of larnite, despite the variation in the experimental temperature, makes TAL an interesting material for CO_2 sequestration [30]. This is because of the presence of Larnite that presents the highest carbonation reaction rate among the calcium silicates, with 64–67 wt.% of CaO, about 50% more than that of wollastonite (42–44 wt.% of CaO), interesting therefore for acting as a possible structural confinement of CO_2 (via Ca-carbonate formation) [3]. The carbonation process is not well documented yet in larnite, although its β-Ca_2SiO_4 phase belite is a major constituent of Portland cement where carbonation is an important process capable to reduce its environmental impact, helping also decrease curing time and increasing materials strength [30].

The slight variations in the starting CDW bulk composition result in different CaO/SiO_2 (C/S) molar ratios in the three samples considered. The higher C/S is in TAL, that is, 2.65, which mainly drives crystallization of the Ca-rich crystal phases that hinder vitrification, although being interesting for possible refractory materials. Even smaller differences in the CaO/SiO_2 (C/S) molar ratio, as 0.75 in PRO versus 0.91 in RAS, produce variations in the mineral and glass formation and temperature of vitrification. Similar studies involving thermal treatments on bottom and fly ashes also demonstrated how low C/S molar ratios facilitate vitrification of the waste samples [6, 31, 32].

These observations parallel similar stability behavior of the main phases, as evidenced by the mineral relations diagrams in Figure 5. In fact, PRO experimental samples show that clinopyroxene (as diopside) is stable at limited temperature and duration conditions (i.e., 1100°C at 2 and 8 h; Figure 5a) while quartz, melilite (gehlenite), and pseudowollastonite are the most stable crystalline phases toward higher temperatures. Glass is then the only stable phase in the 1300°C PRO products.

Similarly, in RAS samples, melilite and wollastonite are stable up to 1300°C, where the only phase present is glass in both the 2- and 8-h duration experiments. Diversely, TAL samples show a distinct behavior, evidenced by the continuous presence of larnite and portlandite up to 1300°C.

3.3 | Design and Optimization of a Value-Added Product

3.3.1 | Experimental Blend (Exp.a)

The first part of this study demonstrated that chemical characterization of CDW samples allows for a detailed prediction of their behavior at high temperature, with bulk compositions close to thermal minima in the $CaO–Al_2O_3–SiO_2$ ternary being most easily vitrified [33]. Building on this, we implement here a computational modeling, which can guide the design of compositions with targeted physical properties starting from waste materials. This information can represent a value-added strategy to determine the upcycling possibility of the PRO sample, whose composition has been identified as the best-vitrifying matrix. To verify the potentials of this waste, it was chosen as the base composition, which was blended with fly ash (FA.REI), to supply a suitable amount of Al_2O_3 and SiO_2, and glass-cutting waste (VF3) (see Tables 3 and 4). These two components are waste materials not usually considered for recycling and thus represent a sustainable addition to the possible recycling of CDW through a vitrification process. An experimental blend (Exp.a; Table 3) was designed and tested to reduce the experimental temperature, with the aim to achieving a more energy-efficient and environmentally sustainable process at the industrial scale, using 100% of waste materials, while simultaneously to develop a new glass with thermomechanical features better than the individual starting waste (PRO, FA.REI, VF3), as discussed in Section 3.3.2. The feasibility of producing this new material was also experimentally validated by mixing the three components using the theoretically calculated proportions and thermally heating the resulting mix at 1230°C for 2 h. The resulting sample is, at macro-appearance,

TABLE 3 | Normalized major chemical compositions (wt.%) and leachates (ppm) of the resulting blend Exp.a.

	SiO_2	Al_2O_3	Fe_2O_3(T)	MnO	MgO	CaO	Na_2O	K_2O	TiO_2	P_2O_5	Total
Exp.a	56.39 (0.52)	13.36 (0.62)	4.57 (0.98)	0.08 (0.02)	2.55 (0.13)	16.24 (0.56)	3.70 (0.16)	1.99 (0.09)	0.65 (0.05)	0.45 (0.05)	100.00
	Li	**Be**	**B**	**Al**	**P**	**Sc**	**Ti**	**V**	**Cr**	**Mn**	**Fe**
	0.000 (0.000)	0.000 (0.000)	0.183 (0.100)	n.d.	n.d.	n.d.	n.d.	0.000 (0.000)	n.d.	0.001 (0.000)	n.d.
	Co	**Sn**	**Ni**	**Cu**	**Zn**	**Ga**	**As**	**Se**	**Rb**	**Sr**	**Mo**
	0.000 (0.000)	0.000 (0.000)	0.001 (0.000)	0.002 (0.001)	0.017 (0.001)	n.d.	0.000 (0.000)	0.000 (0.000)	0.000 (0.000)	0.012 (0.001)	0.000 (0.000)
	Ag	**Cd**	**Sb**	**Te**	**Ba**	**Tl**	**Pb**	**Bi**	**U**		
	0.000 (0.000)	0.000 (0.000)	0.000 (0.000)	n.d.	0.024 (0.001)	0.000 (0.000)	0.000 (0.000)	0.000 (0.000)	n.d.		

Abbreviation: n.d. = not determined.

TABLE 4 | Predicted properties of the starting materials and the final product by using the model GlassNet [18].

	Unit	PRO	FA.REI	VF3	Exp.a
Properties	wt.%	38.59	38.59	22.81	100
Glass transition temperature (T_g)	°C	704.85	773.55	573.73	701.45
Melting temperature (T_m)	°C	1229.44	1344.94	1034.04	1229.44
Liquidus temperature (T_l)	°C	1192.94	1389.74	1055.39	1237.52
Refractive index (n_D)	ad.	1.61	1.57	1.55	1.58
Resistivity 293K	Ω·m	10.65	10.61	10.11	10.51
Young modulus (E)	GPa	58.75	83.21	51.09	66.44
Shear modulus (G)	GPa	37.63	36.43	31.92	35.86
Microhardness (H)	GPa	7.76	9.14	7.63	8.26
Poisson ratio (ν)	ad.	0.24	0.21	0.22	0.22
Density—293K (κ)	$g{\cdot}cm^{-3}$	2.80	2.61	2.65	2.69
Thermal conductivity (k)	$W{\cdot}m^{-1}{\cdot}K^{-1}$	1.47	1.26	1.25	1.34
Thermal shock resistance (ΔT)	°C	155.26	262.72	106.33	185.57
Heat capacity—293K (C_p)	$J{\cdot}kg^{-1}{\cdot}K^{-1}$	801.23	787.19	837.15	804.00

a homogeneous glassy product, confirming that the waste blend can be successfully processed. This is also confirmed at the microscale by the BSE image of the product, which shows that the material presents a glassy matrix, quite uniform (Figure 6), without evident crystals.

Chemical composition of Exp.a (Table 3) show efficient vitrification of the three feedstocks into a single-phase glass. Major oxides exhibit minimal variability: for example, SiO_2 averages 54.97 wt.% with standard deviation (SD) of 0.52 wt.%, while CaO and Al_2O_3 display similarly low SDs of 0.56 and 0.62 wt.%, respectively, suggesting good homogeneity across the experimental sample.

Previous studies regarding glass formation have predominantly focused on the vitrification of single waste feedstocks, such as municipal solid waste residues (e.g., bottom ash, fly ash) [12, 33–35], metallurgical by-products (e.g., copper slag, blast furnace slag) [16, 35, 36, 37, 38], or CDW [3, 6, 7]. For example, [11] reviewed vitrification technologies applied to individual hazardous wastes, primarily aiming at immobilizing contaminants within chemically stable and homogeneous glassy matrices. Furthermore, most studies have concentrated on elucidating the chemical composition, phase assemblage, and microstructural characteristics of the vitrified products, while their thermomechanical performance has not been assessed for their functional potential in new applications.

Therefore, this study can contribute to demonstrating the potential for recycling CDW waste, especially when combined with other waste streams, since recent studies [4, 22, 39] have reported the occurrence of potentially concerning elements (e.g., Cr, Ni, Cu, V, As) in some CDW-derived materials. In this context, leaching tests were carried out on the glass Exp.a to assess the chemical stability and long-term durability of the resulting material under

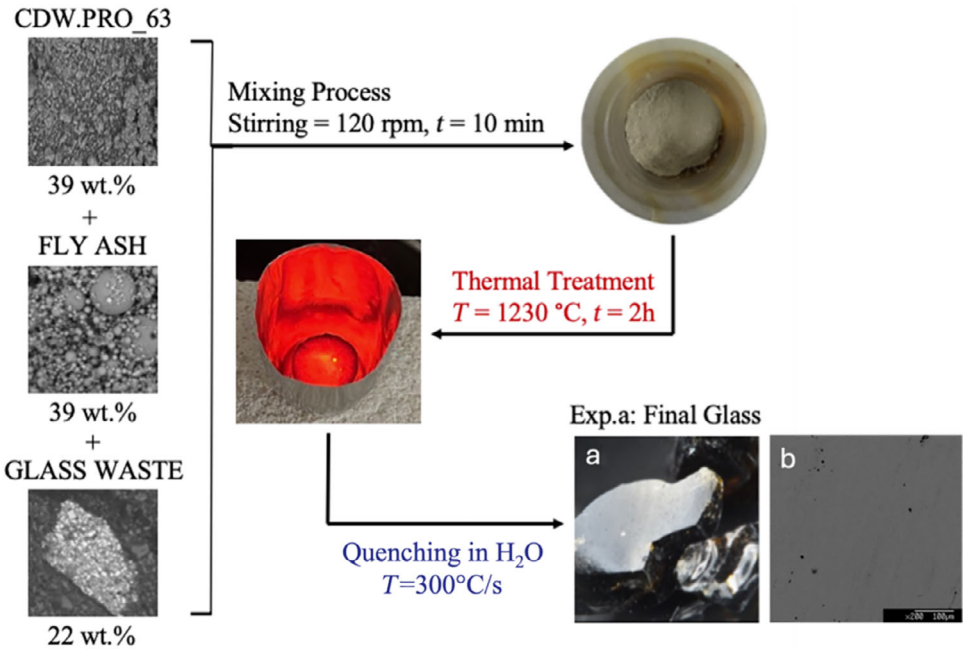

FIGURE 6 | Glass (Exp.a) production process flowchart, also showing, at the bottom right corner of the figure, images of (a) macro appearance and (b) microtexture obtained by BSE of the final product.

environmental conditions, and to verify its compliance with regulatory limits for potential reuse (or, alternatively, disposal in the presence of hazardous components).

The results of the leaching tests, reported in Table 3, indicate that all analyzed elements fall below the corresponding EU regulatory thresholds (EoW) [40], confirming the material's environmental compatibility.

3.3.2 | Thermomechanical Properties

The composition of the Exp.a blend was tested for the definition of thermomechanical properties by a deep neural network GlassNet model [18], widely employed for glass and glass–ceramics properties in literature [41, 42]. In the Python module GlassPy, the model was employed to predict temperature (of melting, T_m; glass transition, T_g; and liquidus, T_l), density (ρ), refractive index (n_D), microhardness (H), elastic moduli (Young's, E; shear, G; and Poisson's ratio, ν), thermal conductivity (k), thermal shock resistance (ΔT), as well as the heat capacity (C_p), of the starting material PRO, coal fly ash FA.REI, and glass-cutting waste VF3. Moreover, the model was used in conjunction with an optimization algorithm to determine the ideal proportions of the three waste materials (Table 4), while maintaining the original melting temperature of PRO ($T_m \approx 1229$°C; Cassar [18]). As demonstrated by [43], lowering the melting temperature could likely lead to a decrease in desired thermomechanical properties. Preserving this melting point ensured, therefore, effective vitrification, while the optimization aimed to improve the thermomechanical properties of the final product.

The optimized composition, referred to as Exp.a, was prepared using 38.6 wt.% PRO, 38.6 wt.% FA.REI, and 22.8 wt.% VF3 (Table 4).

The predicted properties of this optimized blend showed significant improvements over the parent PRO material: the melting temperature was successfully constrained to ~1229°C, and the properties are summarized in Table 4. For instance, elastic properties such as Young's modulus (E) increase from 58.75 to 66.44 GPa, shear modulus (G) and Poisson's ratio (ν) decrease from 37.63 to 35.86 GPa and from 0.24 to 0.22, respectively, going from the pure PRO glassy material to the Exp.a final glass product. This suggests that the resulting material Exp.a deforms less under the same axial load, becomes more flexible and deformable, and is less prone to brittle fracture, an advantage for applications where a reduced bending or breaking behavior is desired. In addition, the thermal conductivity (k) decreases from 1.47 to 1.34 $W \cdot m^{-1} \cdot K^{-1}$, improving the thermal insulation, while the thermal shock resistance (ΔT) increases from 155.26 to 185.57°C, advantageous for the use of glass at high temperature thermal gradients. Moreover, a decrease in density (ρ) from 2.80 to 2.69 $g \cdot cm^3$ makes the resulting materials lighter and more suitable for possible applications as thermal and acoustic insulating material. Literature studies report similar values of density for fiber glasses, in the range of 2.46–2.70 $g \cdot cm^3$, with a focus on wool glass and its potential use for various forms of heat and sound insulation [44]. Further, the decrease in density resulting from the waste adding to the Exp.a blend Exp.a likely reflects a greater degree of structural compaction of the glassy matrix, due mainly to the increase in silica content and decrease in alkaline oxides, thus suggesting that a well-polymerized glass structure could be obtained.

4 | Conclusions

The compositional heterogeneity of CDW makes it difficult to identify it as a constant waste source, hindering its recycling at the industrial level. This happens despite the relevance of this waste stream in EU and in the world, where it is produced by a variety

of processes (building demolition/renovation, natural disasters, human activities including wars). However, in this work, where we focus on the CDW finest fractions (< 0.063 mm), we show that although being usually discarded for the intrinsic difficulty in developing possible applications, they can provide interesting applications and upcycling possibilities.

We demonstrated that the chemical characterization of the fine fractions of CDW, coupled with modeling of thermo-physical and -mechanical properties as a function of composition, can assist the engineering of industrially relevant glassy materials. Results show that higher temperatures and dwell time leads to homgenous glassy materials in two of the samples considered (PRO and RAS), also suggesting their potentiality in immobilize in their stable and homogenous glass structure the heavy metals that are likely present in the starting waste. In contrast, the different chemical composition of TAL (i.e., lower SiO_2 and Al_2O_3 and higher CaO contents compared to the PRO and RAS) inhibited vitrification but demonstrated its potential as refractory treated materials or as CO_2 storage structure.

Moreover, by combining different wastes and by-product streams, with a modeling approach of their thermomechanical properties, it is possible to engineer value-added products that result to be more performant than the PRO sample in terms of flexibility and deformability, as well as for acoustic and thermal-insulating properties. This experimental approach coupled with the modeling of properties can give useful results that fully align with circular economy concepts, emphasizing waste recovery and recycling as key strategies for the rational design and development of advanced materials.

Author Contributions

Roberto Ercoli: conceptualization, formal analysis, investigation, methodology, supervision, validation, visualization, writing – original draft, writing – review and editing. **Paola Stabile:** conceptualization, investigation, supervision, validation, visualization, writing – original draft, writing – review and editing. **Gabriele Giuliani:** investigation, methodology, validation, visualization, writing – original draft, writing – review and editing. **Michael R. Carroll:** visualization, writing – review and editing. **Gianluca Bianchini:** visualization. **Eleonora Paris:** conceptualization, funding acquisition, resources, supervision, validation, visualization, writing – review and editing.

Acknowledgments

Analyses were performed at the EMPA facility of the Unitech COSPECT at the University of Milan (Italy).

Open access publishing facilitated by Universita degli Studi di Camerino, as part of the Wiley - CRUI-CARE agreement.

Funding

This research was funded by PRIN 2022 RUB2RES and Progetto Coesione to E.P., and by PRIN2020 and 202037YPCZ to M.R.C.

Ethics Statement

The authors have nothing to report.

Consent

The authors have nothing to report.

Conflicts of Interest

The authors declare no conflicts of interest.

Data Availability Statement

Data are contained within the article.

References

1. Deloitte, *Study on Resource Efficient Use of Mixed Wastes, Improving Management of Construction and Demolition Waste—Final Report; Prepared for the European Commission DG ENV* (European Commission, 2017).

2. P. Favaretto, G. E. N. Hidalgo, C. H. Sampaio, R. D. A. Silva, and R. T. Lermen, "Characterization and Use of Construction and Demolition Waste From South of Brazil in the Production of Foamed Concrete Blocks," *Applied Sciences* 7 (2017): 1090.

3. A. Abudurehman, P. Stabile, M. R. Carroll, C. Santulli, and E. Paris, "Mineralogical and Chemical Characterization of CDW as Function of Particle Size and Thermal Treatments for Potential Recycling," *Detritus* 15 (2021): 40–50.

4. A. Galderisi, G. Iezzi, G. Bianchini, E. Paris, and J. de Brito, "Petrography of Construction and Demolition Waste (CDW) From Abruzzo Region (Central Italy)," *Waste Management* 137 (2022): 61–71..

5. A. Galderisi, M. Bravo, G. Iezzi, G. Cruciani, E. Paris, and J. Brito, "Physico-Mechanical Performances of Mortars Prepared With Sorted Earthquake Rubble: The Role of CDW Type and Contained Crystalline Phases," *Materials* 16 (2023): 2855..

6. P. Stabile, A. Abudurahman, M. R. Carroll, and E. Paris, "Bulk Composition Effects on Vitrification of Mixed Fine Construction–Demolition and Inorganic Solid Waste," *Minerals* 13 (2023): 1378, https://doi.org/10.3390/min13111378.

7. P. Stabile, L. Fornasini, L. Pasetti, et al., "Characterization of Mixed-Waste Glasses in the CAS System: Insights From Differential Scanning Calorimetry and Raman Spectroscopy," *European Physical Journal Plus* 140 (2025): 739, https://doi.org/10.1140/epjp/s13360-025-06677-3.

8. S. Abidi, B. Nait-Ali, Y. Joliff, and C. Favotto, "Impact of Perlite, Vermiculite and Cement on the Thermal Conductivity of a Plaster Composite Material: Experimental and Numerical Approaches," *Composites Part B: Engineering* 68 (2015): 392–400.

9. M. Jedidi, O. Benjeddou, and C. Soussi, "Effect of Expanded Perlite Aggregate Dosage on Properties of Light Weight Concrete," *Jordan Journal of Civil Engineering* 9 (2015): 378–391.

10. M. J. Whittaker, K. Grigoriadis, S. Soutsos, et al., "Novel Construction and Demolition Waste (CDW) Treatment and Uses to Maximize Reuse and Recycling," *Advances in Building Energy Research* 15 (2019): 253–269.

11. R. C. Sanito, M. Bernuy-Zumaeta, S.-J. You, and Y.-F. Wang, "A Review on Vitrification Technologies of Hazardous Waste," *Journal of Environmental Management* 316 (2022): 115243.

12. P. Stabile, M. Bello, M. Petrelli, E. Paris, and M. R. Carroll, "Vitrification Treatment of Municipal Solid Waste Bottom Ash," *Waste Management* 95 (2019): 250–258..

13. J. S. McCloy and S. Schuller, "Vitrification of Wastes: From Unwanted to Controlled Crystallization, a Review," *Comptes Rendus Géoscience* 354 (2022): 121–160.

14. M. I. Ojovan, "Vitrification as a Key Solution for Immobilisation Within Nuclear Waste Management," *Arabian Journal for Science and Engineering* 50 (2025): 3253–3261, https://doi.org/10.1007/s13369-024-09292-z.

15. P. Zhao, G. Ni, Y. Jiang, L. W. Chen, M. Z. Chen, and Y. D. Meng, "Destruction of Inorganic Municipal Solid Waste Incinerator Fly Ash in a DC Arc Plasma Furnace," *Journal of Hazardous Materials* 181 (2010): 580–585..

16. P. Stabile, F. Vetere, L. Giuliani, et al., "Fabrication of New Glass–Ceramic Materials From Float Glass and Slag Waste by Modulation of the Cooling Rate," *Waste Management* 208 (2025): 115141, https://doi.org/10.1016/j.wasman.2025.115141.

17. D. Caurant, *Glass-Ceramics for Waste Immobilization, in Glass to Crystal Nucleation, Growth and Phase Separation From Research to Applications*, ed. D. Neuville, L. Cormier, D. Caurant, and L. Montagne, (EDP Sciences, 2017), 492–525.

18. D. R. Cassar, "ViscNet: Neural Network for Predicting the Fragility Index and the Temperature-Dependency of Viscosity," *Acta Materialia* 206 (2021): 116602.

19. R. Ercoli, F. Volpintesta, P. Stabile, G. Bianchini, G. Bonifazi, and E. Paris, "A Construction and Demolition Waste (CDW) From Earthquake Rubble to Recycling in Clinker Production: A Chemical-Mineralogical Study Towards Circular Economy and Sustainability," *Journal of Cleaner Production submitted*.

20. H. Putz and K. Brandenburg, *Match!—Phase Analysis Using Powder Diffraction* (Crystal Impact, 2019), https://www.crystalimpact.de/match.

21. B. Lafuente, R. T. Downs, H. Yang, and N. Stone, "The Power of Databases: The RRUFF Project," in *Highlights in Mineralogical Crystallography* (De Gruyter, 2015), 1–30, https://doi.org/10.1515/9783110417104-003.

22. G. Bianchini, I. Ristovski, I. Milcov, et al., "Chemical Characterisation of Construction and Demolition Waste in Skopje City and Its Surroundings (Republic of Macedonia)," *Sustainability* 12, no. 5 (2020): 2055, https://doi.org/10.3390/su12052055.

23. D. A. C. Manning, *Cement and Plasters Industrial Minerals* (Chapman & Hall, 1995), 141–155.

24. G. Bianchini, E. Marrocchino, R. Tassinari, and C. Vaccaro, "Recycling of Construction and Demolition Waste Materials: A Chemical–Mineralogical Appraisal," *Waste Management* 25 (2005): 149–159..

25. F. Volpintesta, E. Ossoli, A. Reggiani, P. Stabile, C. Santulli, and E. Paris, "Geopolymers-Based Application for the Up-Cycling Utilization of Construction and Demolition Waste From the 2016 Central Italy Earthquakes," *Materials Letters* 336 (2023): 133849.

26. R. H. Hand, "Soda-Lime-Silica Glasses," in *Encyclopedia of Materials: Technical Ceramics and Glasses*, ed. M. Pomeroy, (Elsevier, 2021), 483–495.

27. S. Milani, D. Comboni, P. Lotti, et al., "Crystal Structure Evolution of CaSiO3 Polymorphs at Earth's Mantle Pressures," *Minerals* 11 (2021): 652, https://doi.org/10.3390/min11060652.

28. K. Schollbach, Q. Alam, V. Caprai, et al., "Combined Characterization of the MSWI Bottom Ash," in *Proceedings of the Thirty-Eighth International Conference On Cement Microscopy* (International Cement Microscopy Association, 2016).

29. N. Yamnova, N. Zubkova, N. Eremin, A. Zadov, and V. Gazeev, "Crystal Structure of Larnite β-Ca 2SiO 4 and Specific Features of Polymorphic Transitions in Dicalcium Orthosilicate," *Crystallography Reports* 56 (2011): 210–220, https://doi.org/10.1134/S1063774511020209.

30. A. Santos, M. Ajbary, V. Morales-Flores, A. Kherbeche, M. Pinero, and L. Esquivias, "Larnite Powders and Larnite/Silica Aerogel Composites as Effective Agent for CO2 Sequestration by Carbonation," *Journal of Hazardous Materials* 168 (2009): 1397–1403..

31. S. Kucharczyk, M. Sitarz, M. Zajac, and J. Deja, "The Effect of CaO/SiO2 Molar Ratio of CaO-Al2O3-SiO2 Glasses on Their Structure and Reactivity in Alkali Activated System, Spectrochim," *Spectrochimica Acta Part A: Molecular and Biomolecular Spectroscopy* 194 (2018): 163–171, https://doi.org/10.1016/j.saa.2018.01.018.

32. E. Sharifikolouei, F. Baino, M. Salvo, et al., "Vitrification of Municipal Solid Waste Incineration Fly Ash: An Approach to Find the Successful Batch Compositions," *Ceramics International* 47, no. 6 (2021): 7738–7744, https://doi.org/10.1016/j.ceramint.2020.11.118.

33. K. Maeda, K. Akatsuka, G. Okuma, and A. Yasumori, "Mechanical Properties of $CaO–Al_2O_3–SiO_2$ Glass-Ceramics Precipitating Hexagonal $CaAl_2Si_2O_8$ Crystals," *Crystals* 11, no. 4 (2021): 393, https://doi.org/10.3390/cryst11040393.

34. C. H. Jung and M. Osako, "Thermodynamic Behaviour of Rare Metals in the Melting Process of Municipal Solid Waste (MSW) Incineration Residues," *Chemosphere* 69 (2007): 279–288..

35. T. Sekito, Y. Dote, K. Onoue, H. Sakanakura, and K. Nakamura, "Characteristics of Element Distributions in an MSW Ash Melting Treatment System," *Waste Management* 34, no. 9 (2014): 1637–1643, https://doi.org/10.1016/j.wasman.2014.04.009.

36. S. Deng, C. Li, H. Guo, W. Zhao, B. Yan, and P. Li, "Crystallization Characteristics, Microstructural Evolution, and Cr Migration Mechanism of Glass-Ceramics Synthesized Entirely From Low-Carbon Ferrochromium Slag and Waste Glass," *Journal of Hazardous Materials* 445 (2023): 130621, https://doi.org/10.1016/j.jhazmat.2022.130621..

37. L. Liu, H. Yu, Y. Li, and Z. Zhang, "Stabilization Behavior and Mechanism of Heavy Metals in Eco-Friendly Glass-Ceramics Derived From Wastes," *Journal of Cleaner Production* 269 (2020): 122417, https://doi.org/10.1016/j.jclepro.2020.122417.

38. W. Shang, Z. Peng, Y. Huang, et al., "Production of Glass-Ceramics From Metallurgical Slags," *Journal of Cleaner Production* 317 (2021): 128220, https://doi.org/10.1016/j.jclepro.2021.128220.

39. A. Bisciotti, V. Brombin, Y. Song, G. Bianchini, and G. Cruciani, "Classification and Predictive Leaching Risk Assessment of Construction and Demolition Waste Using Multivariate Statistical and Machine Learning Analyses," *Waste Management* 196 (2025): 60–70..

40. K. A. Villanueva and P. Eder, "End-of-Waste Criteria for Wastepaper: Technical Proposals," in *EUR 24789 EN* (Publications Office of the European Union, 2011).

41. R. A. Silva, G. Batista, R. Cassani, et al., "Thermal, Chemical, and Mechanical Properties of Niobium Phosphate Glasses and Glass-Ceramics," *Ceramics International* 50, no. 11 Part A (2024): 18618–18627.

42. F. Pigeonneau, M. Rondet, O. De Lataulade, and E. Hachem, "Physical-Informed Deep Learning Prediction of Solid and Fluid Mechanical Properties of Oxide Glasses," *Journal of Non-Crystalline Solids* 657 (2025): 123476.

43. T. Rouxel, "Elastic Properties and Short-to Medium-Range Order in Glasses," *Journal of the American Ceramic Society* 90 (2007): 3019–3039.

44. K. H. J. Buschow, R. W. Cahn, M. C. Flemings, B. Ilschner, E. J. Kramer, and S. Mahajan, *Encyclopedia of Materials: Science and Technology* (Elsevier, 2001).